Dioxygen Cleavage and Methane Activation on Diiron Enzyme Models: A Theoretical Study

Kazunari Yoshizawa,*,† Takehiro Ohta,† Tokio Yamabe,†,‡ and Roald Hoffmann*,§

Contribution from the Department of Molecular Engineering, Kyoto University, Sakyo-ku, Kyoto 606-01, Japan, Institute for Fundamental Chemistry, 34-4 Takano-Nishihiraki-cho, Sakyo-ku, Kyoto 606, Japan, and Department of Chemistry, Cornell University, Ithaca, New York 14853-1301

Received August 1, 1997. Revised Manuscript Received October 6, 1997[⊗]

Abstract: Two possible mechanisms for dioxygen cleavage on non-heme diiron enzyme models are studied with an approximate molecular orbital method, the extended Hückel method. Diiron peroxo model complexes with different μ-η^1:η^1-O_2 and μ-η^2:η^2-O_2 binding modes are distorted to corresponding dioxo complexes along an assumed O−O bond cleavage reaction coordinate. Fragment molecular orbital (FMO) and Walsh diagram analyses clarify the bonding and orbital interactions. While the π_g* orbitals of O_2 are initially occupied by two electrons, in the first dioxygen binding step two other electrons are effectively transferred from the "t_{2g}" block to O_2 to form O_2^{2-}. To cleave the dioxygen O−O bond, it is necessary further to fill the σ_u* orbital (high lying and unoccupied in the peroxide). The computations suggest that the μ-η^1:η^1-O_2 mode is more effective for electron transfer from the d-block orbitals to the σ_u*. Our calculations indicate that a C_{3v}- or D_{2d}-distorted methane can be activated if a coordinatively unsaturated iron, which has been proposed to exist in the diamond $Fe_2(\mu\text{-}O)_2$ core of intermediate **Q** of methane monooxygenase, is generated. The complex is suggested to include a five-coordinate carbon species with an Fe−CH_4 bond. We propose possible concerted reaction pathways for the conversion of methane to methanol on the supposed diiron active site of methane monooxygenase. Inversion at a five-coordinate carbon species is suggested to reasonably occur in an initially formed complex of methane and a model of intermediate **Q**, leading to inversion of stereochemistry at a labeled carbon center.

Introduction

Cleavage of the dioxygen O−O bond figures most importantly in the catalytic cycles of various oxygen-activating metalloenzyme systems. Oxygen transport and storage and oxidation of organic substrates take place at the active sites of non-heme diiron enzymes. For example, hemerythrin (Hr) in marine invertebrates binds dioxygen reversibly at its diiron active site in a manner comparable to the mammalian proteins myoglobin and hemoglobin;[1,2] methane monooxygenase (MMO) converts the most inert hydrocarbon, methane, into methanol;[1,2] and ribonucleotide reductase (RR) reduces ribo- to deoxyribonucleotides in the early stages of DNA biosynthesis.[1,2]

The relevant active sites of metalloenzymes with a non-heme diiron core structure are shown in Figure 1. The dioxygen binding mode in Hr is well established from X-ray structural analyses.[2] Although crystal structures of MMO and RR are now available both in the diiron(II) and diiron(III) states, the structures of the bound peroxo forms of MMO and RR are still the subject of debate. The roles of MMO and RR are quite different, in spite of their structural similarities at the respective active sites.

The catalytic processes of these iron-based metalloenzymes are likely to be initiated by two important reactions involving dioxygen. The first of these is initial binding of O_2 to a diiron active site, forming a peroxo species; the second is an O−O bond cleaving step. In the catalytic action of metalloenzymes, heterolytic cleavage of the O−O bond of dioxygen bound to a transition metal active site is supposed to occur. For instance, in a proposed catalytic mechanism for cytochrome P450 (which is able to hydroxylate a variety of hydrocarbons),[3] the O−O bond is cleaved at the heme iron to produce a diatomic unit which may be written as $Fe^{III}-O^0$, $Fe^{IV}-O^-$, or $Fe^{V}-O^{2-}$. The π system of the porphyrin ring may also be oxidized to a cation radical; as a result, the so-called "compound I", with an $Fe^{III}-O^-$ or $Fe^{IV}=O^{2-}$ core structure, is formed. This species is postulated to directly abstract a hydrogen atom from hydrocarbons, to form a substrate radical and an iron-coordinated hydroxy radical. The two radical species are then thought to recombine in a *rebound* mechanism to afford product alcohol.[3]

Although cytochrome P450 cannot hydroxylate methane, MMO can convert this most inert hydrocarbon to methanol under physiological conditions.[4−9] The role of the diiron active

† Kyoto University.
‡ Institute for Fundamental Chemistry.
§ Cornell University.
⊗ Abstract published in *Advance ACS Abstracts,* December 1, 1997.

(1) (a) *Mechanistic Bioinorganic Chemistry*; Thorp, H. H., Pecoraro, V. L., Eds.; American Chemical Society: Washington, DC, 1995. (b) Bertini, I.; Gray, H. B.; Lippard, S. J.; Valentine, J. S. *Bioinorganic Chemistry*; University Science Books: California, 1994. (c) Lippard, S. J.; Berg, J. M. *Principles of Bioinorganic Chemistry*; University Science Books: California, 1994. (d) Kaim, W.; Schwederski, B. *Bioinorganic Chemistry: Inorganic Elements in the Chemistry of Life*; Wiley: New York, 1994. (e) Fraústo da Silva, J. J. R.; Williams, R. J. P. *The Biological Chemistry of the Elements*; Clarendon: Oxford, 1991.

(2) Recent reviews on non-heme diiron enzymes: (a) Kurtz, D. M., Jr. *J. Biol. Inorg. Chem.* **1997**, *2*, 159. (b) Wallar, B. J.; Lipscomb, J. D. *Chem. Rev.* **1996**, *96*, 2625. (c) Que, L., Jr.; Dong, Y. *Acc. Chem. Res.* **1996**, *29*, 190. (d) Feig, A. L.; Lippard, S. J. *Chem. Rev.* **1994**, *94*, 759. (e) Stenkamp, R. E. *Chem. Rev.* **1994**, *94*, 715. (f) Lipscomb, J. D. *Annu. Rev. Microbiol.* **1994**, *48*, 371. (g) Vincent, J. B.; Oliver-Lilley, G. L.; Averill, B. A. *Chem. Rev.* **1990**, *90*, 1447. (h) Kurtz, D. M., Jr. *Chem. Rev.* **1990**, *90*, 585. (i) Lippard, S. J. *Angew. Chem., Int. Ed. Engl.* **1988**, *27*, 344. (j) Wilkins, P. C.; Wilkins, R. G. *Coord. Chem. Rev.* **1987**, *79*, 195.

(3) *Cytochrome P450: Structure, Mechanism, and Biochemistry*, 2nd ed.; Ortiz de Montellano, P. R., Ed.; Plenum: New York, 1995.

(4) Green, J.; Dalton, H. *J. Biol. Chem.* **1989**, *264*, 17698.

(5) Ruzicka, F.; Huang, D. S.; Donnelly, M. I.; Frey, P. A. *Biochemistry* **1990**, *29*, 1696.

(6) Rataj, M. J.; Knauth, J. E.; Donnelly, M. I. *J. Biol. Chem.* **1991**, *266*, 18684.

S0002-7863(97)02641-3 CCC: $14.00

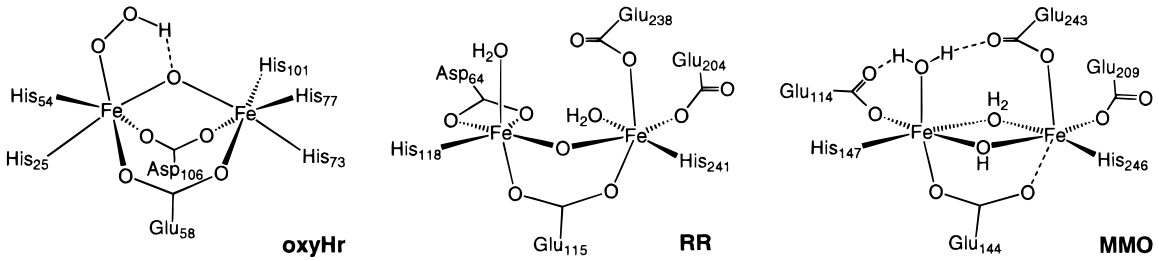

Figure 1. Diiron active centers of oxyhemerythrin (oxyHr), ribonucleotide reductase (RR), and methane monooxygenase (MMO).

Scheme 1

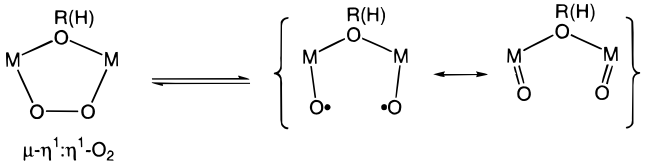

Scheme 2

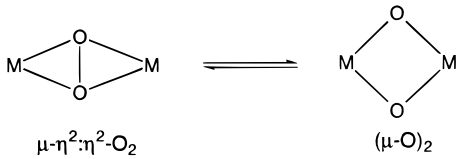

site in this unique function of MMO has been of interest to us. A peroxo form with a μ-η^1:η^1-O_2 binding mode (*cis*- and *trans*-μ-1,2-O_2 mode) has been suggested crystallographically[10−12] and theoretically[13,14] to play a role in the initial stages of the catalytic cycle of MMO. In both approaches, model systems were used; the structure of the actual peroxo-bound form of MMO is still unknown. The importance of homolytic cleavage of bound dioxygen for activating an oxidative reaction in a dinuclear iron model complex has been emphasized, as indicated in Scheme 1.[11] The decay rate of the intermediate is modulated by the introduction of substituents and correlates with Hammett σ values.

The μ-η^1:η^1-O_2 binding mode mentioned above is one possibility for the peroxo-bound forms of MMO and RR. But there is a potential alternative—the μ-η^2:η^2-O_2 mode indicated in Scheme 2. This core structure has been crystallographically well established for dicopper complexes, in the structures of oxyhemocyanin and synthetic analogues.[15−18] Tolman and Que and their collaborators[19] demonstrated through a dicopper model complex similar to hemocyanin that there is an interesting equilibrium between $[Cu(\mu\text{-}\eta^2\text{:}\eta^2\text{-}O_2)]^{2+}$ and $[Cu_2(\mu\text{-}O)_2]^{2+}$ modes. This equilibrium is shifted toward a μ-η^2:η^2-O_2 core structure in dichloromethane, while in tetrahydrofuran a $(\mu$-$O)_2$ core structure is favored. Recent *ab initio* calculations[20] indicated that dicopper model complexes with μ-η^2:η^2-O_2 and $(\mu$-$O)_2$ cores are very close in energy, but the dioxo forms are better solvated than the peroxo forms with a μ-η^2:η^2-O_2 mode, by 5.6 to 8.4 kcal/mol. Extended Hückel MO analyses of the reversible transformation in a dicopper model system were carried out.[21] To the best of our knowledge, diiron peroxo complexes with a μ-η^2:η^2-O_2 core structure are not yet known, in contrast to dicopper systems.

The reverse reaction to the dioxygen cleavage, oxidative coupling of oxides derived from water molecules to produce O_2, occurs at a tetranuclear manganese cluster proposed to consist of two $Mn_2(\mu$-$O)_2$ components in photosystem II.[22] Possible mechanisms for O_2 evolution in this system have been studied in terms of orbital interactions by Proserpio, Hoffmann, and Dismukes.[23]

Cleavage of the dioxygen O−O bond at the dimetal site of metalloenzymes is clearly a pivotal process in the catalytic cycle of oxygen-activating metalloenzymes. Theoretical analyses of the O_2-activating process may be useful in clarifying the metal-specialized functions of Hr, RR, and MMO in Figure 1. The purpose of this paper is to analyze the general features of dioxygen O−O bond cleavage and methane activation at diiron active sites, and to explore theoretically the reactivities of peroxo forms and corresponding O···O nonbonded dioxo forms, especially in the context of understanding the enzymatic function of methane monooxygenase (MMO). We examine two quite different reaction pathways, leading from diiron peroxo complexes with μ-η^1:η^1-O_2 and μ-η^2:η^2-O_2 modes to the corresponding dioxo model complexes. Moreover, we propose novel two-step mechanisms that include concerted hydrogen and

(7) Priestley, N. D.; Floss, H. D.; Froland, W. A.; Lipscomb, J. D.; Williams, P. G.; Morimoto, H. *J. Am. Chem. Soc.* **1992**, *114*, 7561.
(8) (a) Liu, K. E.; Johnson, C. C.; Newcomb, M.; Lippard, S. J. *J. Am. Chem. Soc*. **1993**, *115*, 939. (b) Liu, K. E.; Valentine, A. M.; Wang, D.; Huynh, B. H.; Edmondson, D. E.; Sailfoglou, A.; Lippard, S. J. *J. Am. Chem. Soc.* **1995**, *117*, 10174. (c) Liu, K. E.; Valentine, A. M.; Qiu, D.; Edmondson, D. E.; Appelman, E. H.; Spiro, T. G.; Lippard, S. J. *J. Am. Chem. Soc.* **1995**, *117*, 4997. (d) Liu, K. E.; Wang, D.; Huynh, B. H.; Edmondson, D. E.; Salifoglou, A.; Lippard, S. J. *J. Am. Chem. Soc.* **1994**, *116*, 7465.
(9) (a) Rosenzweig, A. C.; Frederick, C. A.; Lippard, S. J.; Nordlund, P. *Nature* **1993**, *366*, 537. (b) Rosenzweig, A. C.; Nordlund, P.; Takahara, P. M.; Frederick, C. A.; Lippard, S. J. *Chem. Biol.* **1995**, *2*, 409.
(10) Ookubo, T.; Sugimoto, H.; Nagayama, T.; Masuda, H.; Sato, T.; Tanaka, K.; Maeda, Y.; Okawa, H.; Hayashi, Y.; Uehara, A.; Suzuki, M. *J. Am. Chem. Soc*. **1996**, *118*, 701.
(11) Dong, Y.; Shiping, Y.; Young, V. G., Jr.; Que, L., Jr. *Angew. Chem., Int. Ed. Engl.* **1996**, *35*, 618.
(12) Kim, K.; Lippard, S. J. *J. Am. Chem. Soc.* **1996**, *118*, 4914.
(13) Yoshizawa, K.; Hoffmann, R. *Inorg. Chem.* **1996**, *35*, 2409.
(14) Yoshizawa, K.; Yamabe, T.; Hoffmann, R. *New J. Chem.* **1997**, *21*, 151.
(15) Kitajima, N.; Fujisawa, K.; Fujimoto, C.; Moro-oka, Y.; Hashimoto, S.; Kitagawa, T.; Toriumi, K.; Tatsumi, K.; Nakamura, A. *J. Am. Chem. Soc.* **1992**, *114*, 1277.
(16) (a) Ross, P. K.; Solomon, E. I. *J. Am. Chem. Soc.* **1991**, *113*, 3246. (b) Solomon, E. I.; Baldwin, M. J.; Lowery M. D. *Chem. Rev.* **1992**, *92*, 521. (c) Solomon, E. I.; Tuczek, F.; Root, D. E.; Brown, C. A. *Chem. Rev.* **1994**, *94*, 827. (d) Solomon, E. I.; Lowery M. D. *Science* **1993**, *259*, 1575. (e) Tuczek, F.; Solomon, E. I. *Inorg. Chem.* **1992**, *31*, 944. (f) Tuczek, F.; Solomon, E. I. *Inorg. Chem.* **1993**, *32*, 2850.
(17) Ling, J.; Nestor, L. P.; Czernuszewicz, R. S.; Spiro, T. G.; Fraczkiewicz, R., Sharma, K. D.; Loehr, T. M.; Sanders-Loehr, J. *J. Am. Chem. Soc.* **1994**, *116*, 7682.
(18) Magnus, K. A.; Hazes, B.; TonThat, H.; Bonaventura, C.; Bonaventura, J.; Hol, W. G. J. *Proteins* **1994**, *19*, 302.
(19) Halfen, J. A.; Mahapatra, S.; Wilkinson, E. C.; Kaderli, S.; Young, V. G., Jr.; Que, L., Jr.; Zuberbühler, A. D.; Tolman, W. B. *Science* **1996**, *271*, 1397.
(20) Cramer, C. J.; Smith, B. A.; Tolman, W. B. *J. Am. Chem. Soc.* **1996**, *118*, 11283.
(21) Yoshizawa, K.; Ohta, T.; Yamabe, T. *Bull. Chem. Soc. Jpn*. **1997**, *70*, 1911.
(22) (a) Pecoraro, V. L.; Baldwin, M. J.; Gelasco, A. *Chem. Rev*. **1994**, *94*, 807. (b) Sauer, K.; Yachandra, V. K.; Britt, R. D.; Klein, M. P. In *Manganese Redox Enzymes;* Pecoraro, V. L. Ed.; VCH: New York, 1992. (c) Yachandra, V. K.; DeRose, V. J.; Latimer, M. J.; Mukerji, I.; Sauer, K.; Klein, M. P. *Science* **1993**, *260*, 675. (d) Wieghardt, K. *Angew. Chem., Int. Ed. Engl*. **1989**, *28*, 1153.
(23) Proserpio, D. M.; Hoffmann, R.; Dismukes, G. C. *J. Am. Chem. Soc.* **1992**, *114*, 4374.

Scheme 3

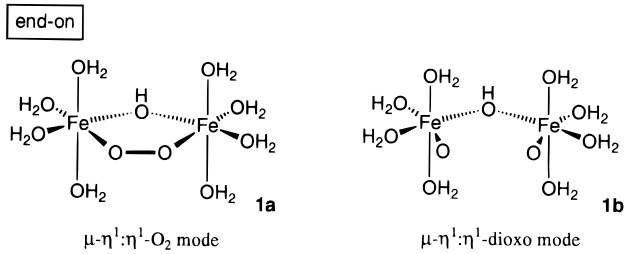

Scheme 4

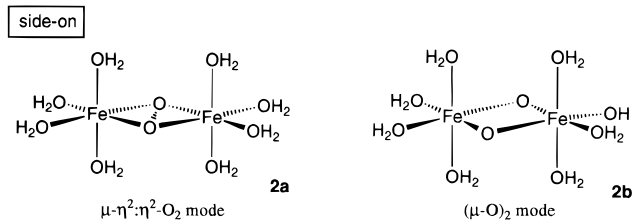

methyl migrations for the conversion of methane to methanol on a diiron active site of intermediate **Q**. This intermediate reacts directly with methane to afford methanol[2b] through a still unknown reaction mechanism. Que and Lipscomb and their co-workers[24] have very recently determined from EXAFS and Mössbauer analyses that intermediate **Q** has the structural and electronic features consistent with a high-valent $Fe_2(\mu\text{-}O)_2$ diamond core structure. Finally, inversion of the five-coordinate carbon species through a planar D_{4h} structure is discussed.

Diiron Enzyme Models

Consider the two types of end-on and side-on O_2 coordination (**1** and **2**), indicated in Schemes 3 and 4. The **a** and **b** symbols in these illustrations distinguish peroxo and related dioxo forms, respectively. **1a** in Scheme 3 models a peroxo complex with a $\mu\text{-}\eta^1\text{:}\eta^1\text{-}O_2$ core structure. This type of peroxo-bridged diiron(III) model complex, which can be classified as a *cis*-μ-1,2-O_2 mode, has been crystallographically established recently in the research groups of Suzuki[10] and Que.[11] The $\mu\text{-}\eta^1\text{:}\eta^1\text{-}O_2$ (*cis*-μ-1,2-) binding mode was proposed by two of us[13] to be energetically preferred to $\mu\text{-}\eta^2\text{:}\eta^2\text{-}O_2$ and μ-1,1-O_2 modes for a hypothetical MMO active site in which one of the monodentate bridging ligands (water or hydroxy) is removed from the molecular structure of MMO,[9b] as shown above in Figure 1.

The terminal ligands of the models in Scheme 3 were modeled by water. We set the Fe−O(water) distances as 2.1 Å, the Fe−O(hydroxy) distances as 2.0 Å, and the Fe−O(peroxy) as 1.9 Å. The resultant Fe···Fe nonbonded distance is then 3.46 Å. The O−O distances for the peroxo and dioxo forms were assumed to be 1.4 Å and 2.4 Å, respectively. The O(equatorial)−Fe−O(equatorial) angles were taken as 87.5° and those of O(equatorial)−Fe−O(hydroxy) as 87.5°. These bond angles were actually optimized with the extended Hückel method, which generally does not give good distances but models bond angles and dihedral angles adequately. Models **1a** and **1b** have C_{2v} symmetry. Since the two irons and the hydroxy bridge have charge +2 and −1, respectively, the total charge on **1a** or **1b** is +3.

On the basis of spectroscopic studies, a peroxo form of type **1a** or a modified form with a *trans*-μ-1,2-O_2 bridging mode has been proposed as one possible structure for a first intermediate ("**P**" or "H_{peroxo}") in the catalytic cycle of MMO.[8b,c,12] A dioxo form of type **1b**, derived from homolytic cleavage of the O−O bond in a peroxo form, is one of the structures that Lippard and co-workers[8b,d] proposed for a second intermediate **Q** in the catalytic cycle of MMO.

Model **2a** in Scheme 4 is a peroxo model with a planar diiron $\mu\text{-}\eta^2\text{:}\eta^2\text{-}O_2$ mode. As observed by Raman spectroscopy, the O−O frequency in the $\mu\text{-}\eta^2\text{:}\eta^2\text{-}O_2$ bridging geometry in dicopper complexes[15,16] and the η^2-O_2 mode in iron porphyrin[25−27] is near 800 cm^{-1}, which is significantly lower than the observed frequency of about 900 cm^{-1} in a peroxo model complex[12,28] with a $\mu\text{-}\eta^1\text{:}\eta^1\text{-}O_2$ mode and intermediate **P** of MMO.[8c] Que et al.[29] synthesized high-valent model complexes with a bis(μ-oxo)diiron core structure, which can be modeled by **2b**; moreover, **2b** is a good model for the $Fe_2(\mu\text{-}O)_2$ diamond core detected in intermediate **Q**,[24] except for the coordination sphere. **Q** is suggested to contain two five- or four-coordinate Fe(IV) atoms.

Let us first assume that each iron is in an octahedral environment, and look at essential orbital interactions in these binding modes. The terminal ligands of these molecules are similarly modeled by water. In models **1** and **2**, we did not include a carboxylate ligand bridge that all the active sites of the diiron metalloenzymes in Figure 1 contain. This is because in the Walsh diagram leading from **2a** to **2b** it is difficult to describe a reaction coordinate for O−O bond cleavage with a single parameter if a carboxylate bridge is retained. Orbital considerations indicate that such a bridge is unlikely to affect level patterns and energetics. We set the Fe−O(bridge) distances as 1.92 Å and the Fe−O(water) as 2.1 Å. The O(axial)−Fe−O(equatorial) and O(equatorial)−Fe−O(equatorial) angles were optimized by the extended Hückel method to be 90° and 80°, respectively. The O−O distances in the peroxo and dioxo forms are assumed as 1.4 and 2.4 Å, respectively. The Fe···Fe distances for **2a** and **2b** then are 3.58 and 2.68 Å, respectively. These models have D_{2h} symmetry. Since the two irons have charge +2, the total charges of **2a** and **2b** are +4.

We study the general electronic features of **1a**, **1b**, **2a**, and **2b** with the extended Hückel method.[30] Levels are calculated and then filled with electrons. This approximate molecular orbital method is not reliable for bonding energies and spin systematics, but should model reasonably well general orbital energy trends, orbital interactions, and major charge shifts.

Dioxygen Cleavage Starting from the End-On $\mu\text{-}\eta^1\text{:}\eta^1\text{-}O_2$ Core

In our previous papers,[13,14] we used a diiron model complex bridged by a bidentate carboxylate group, whose electronic structure is not essentially different from that of our new model **1a**. To understand the governing orbital interactions, we

(24) Shu, L.; Nesheim, J. C.; Kauffmann, K.; Münck, E.; Lipscomb, J. D.; Que, L., Jr. *Science* **1997**, *275*, 515.

(25) (a) McCandlish, E.; Miksztal, A. R.; Nappa, M.; Sprenger, A. G.; Valentine, J. S.; Stong, J. D.; Spiro, T. G. *J. Am Chem. Soc.* **1980**, *102*, 4268.

(26) Burstyn, J. N.; Roe, J. A.; Miksztal, A. R.; Shaevitz, B. A.; Lang, G.; Valentine, J. S. *J. Am. Chem. Soc.* **1988**, *110*, 1382.

(27) Ahmad, S.; McCallum, J. D.; Shiemke, A. K.; Appelman, E. H.; Loehr, T. M.; Sanders-Loehr, J. *Inorg. Chem.* **1988**, *27*, 2230.

(28) (a) Menage, S.; Brennan, B. A.; Juarez-Garcia, C.; Münck, E.; Que, L., Jr. *J. Am. Chem. Soc.* **1990**, *112*, 6423. (b) Dong, Y.; Menage, S.; Brennan, B. A.; Elgren, T. E.; Jang, H. G.; Pearce, L. L.; Que, L., Jr. *J. Am. Chem. Soc.* **1993**, *115*, 1851.

(29) (a) Zang, Y.; Pan, G.; Que, L., Jr. *J. Am. Chem. Soc.* **1994**, *116*, 3653. (b) Zang, Y.; Dong, Y.; Que, L., Jr.; Kauffmann, K.; Münck, E. *J. Am. Chem. Soc.* **1995**, *117*, 1169. (c) Dong, Y.; Fujii, H.; Hendrich, M. P.; Leising, R. A.; Pan, G.; Randall, C. R.; Wilkinson, E. C.; Zang, Y.; Que, L., Jr.; Fox, B. G.; Kauffmann, K.; Münck, E. *J. Am. Chem. Soc.* **1995**, *117*, 2778.

(30) *YAeHMOP*. Landrum, G. Cornell University: Ithaca, New York, 1995. See (a) Hoffmann, R. *J. Chem. Phys.* **1963**, *39*, 1397. (b) Hoffmann, R.; Lipscomb, W. N. *J. Chem. Phys.* **1962**, *36*, 2179; *37*, 2872.

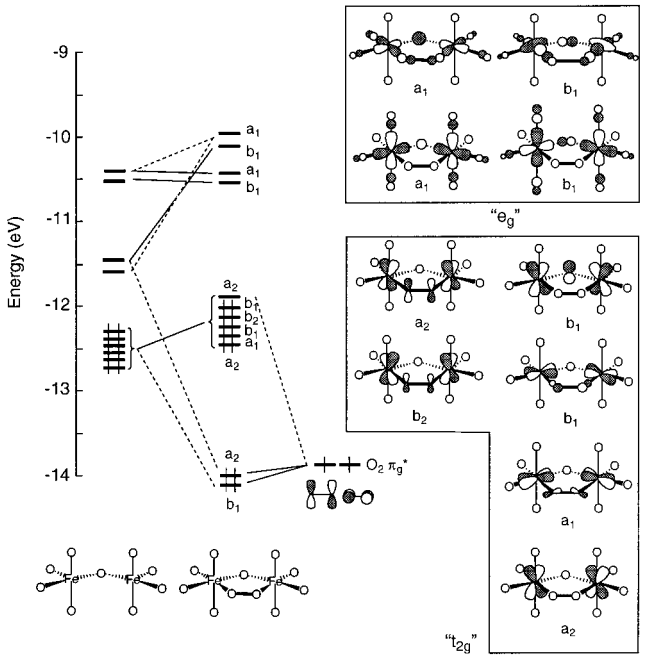

Figure 2. Orbital interaction diagram for diiron peroxo model with a μ-η^1:η^1-O_2 core structure (**1a**).

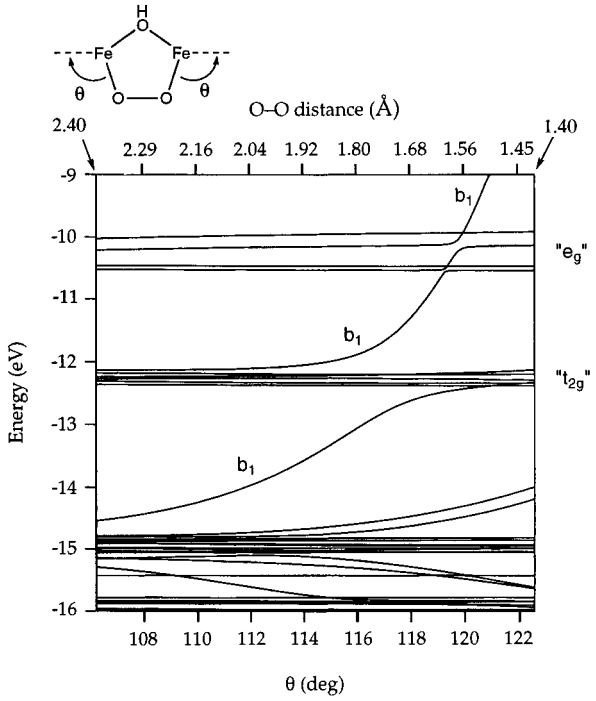

Figure 3. Walsh diagram for model **1a** as a function of O−O distance.

partition the peroxo model complex into one fragment composed of the diiron active site model, and another consisting of just the dioxygen. The bonding in **1a** is then constructed as in Figure 2. There are two nonbonding frontier orbitals near −11.5 eV in the active site of the diiron fragment, indicated at left in Figure 2. One of these nonbonding orbitals (the out-of-phase combination) interacts strongly with the 2-fold degenerate dioxygen π_g* to form the upper b_1 of the "e_g" block. The in-phase combination interacts with dioxygen π_u, which is below the energy window of the illustration, to form the a_1 of the "e_g" block. These antibonding combinations are pushed up significantly, to −10 eV.

Some of the "t_{2g}" orbitals also interact weakly with the dioxygen π_g*. Since the π_g* is lower in energy than the iron d orbitals, the resulting in-phase combination after interaction will have more oxygen π_g* than metal d character. And it will be occupied by electrons. Thus, while the π_g* orbitals of O_2 begin in the neutral diatomic with two electrons, two or more electrons are effectively transferred from the "t_{2g}" block of the dimetal fragment to O_2, to form O_2^{2-}. In this bound peroxo form, there is still one O_2 orbital (the antibonding σ_u*) that is not occupied. The bond order of the peroxide is thus effectively 1; to cleave the dioxygen O−O bond completely it is necessary to fill the antibonding σ_u* orbital by two electrons.

In the next step in the catalytic cycles, cleavage of the peroxide O−O bond is supposed to occur. This important step, experimentally not yet well defined, is represented in our model complexes by the reaction pathway from **1a** to **1b**. One way to pull the two oxygen atoms apart is to change the O(equatorial)−Fe−O(peroxy) angles, keeping other bond lengths and angles constant. In Figure 3 we show the Walsh diagram for the distortion from **1a** to **1b** as a function of the angle defined in the figure. The resulting O−O distance is also given.

Since the two irons are in a nearly octahedral environment, there are six "t_{2g}" block orbitals at −12.1 to −12.3 eV and four "e_g" block orbitals at −10.0 to −10.5 eV. This "six-below-four" d-orbital splitting pattern is typical for octahedral binuclear complexes in which the metal atoms interact weakly.[31] The six "t_{2g}" block orbitals are to be occupied by 10 electrons; the lower five orbitals could be doubly occupied in a singlet state. An alternative, competing configuration would be a triplet.

Scheme 5

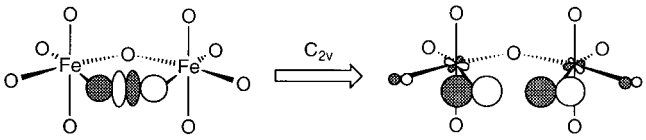

When we look at the Walsh diagram from right to left, a b_1 orbital goes down across the "e_g" and "t_{2g}" block orbitals, although as a consequence of the symmetry a crossing with these orbitals is avoided. This is the σ_u* orbital of dioxygen. The σ_u* (b_1) orbital of the peroxo form **1a**, which is located at −6 eV (outside the energy window of Figure 3) is indicated at left in Scheme 5. As the O−O bond is stretched, the σ_u* orbital falls in energy. The π_g* set (a_2 and b_1) is not as dramatically changed by the distortion, because of weak π-type interactions. These two orbitals are always occupied in this diagram. These levels (at ∼−14 eV) are slightly pushed down, to −14.8 eV, as the O−O distance is increased from 1.4 to 2.4 Å.

In order to break the O−O bond of the peroxide, the b_1 (σ_u*) orbitals must become occupied, as mentioned above. The antibonding interactions in the b_1 (σ_u*) orbital are significantly decreased with an increase in the O−O bond length; the orbital falls to −14.5 eV when the O−O distance becomes 2.4 Å in our dioxide model, **1b**. As a consequence, two more electrons are effectively transferred from the "t_{2g}" block to the σ_u* orbital, to create $2O^{2-}$. In fact, the computed charge of one oxygen of the dioxo form is −1.62 while that of the peroxo form is −0.55.

Dioxygen Cleavage Starting from the Side-On μ-η^2:η^2-O_2 Core

In Figure 4, the orbital interactions building up a diiron peroxo model having a μ-η^2:η^2-O_2 core structure (**2a**) are indicated. The complex is partitioned into $Fe_2(H_2O)_8$ and O_2 fragments. The $Fe_2(H_2O)_8$ fragment has four nonbonding orbitals, in contrast to the $Fe_2(H_2O)_8(OH)$ fragment in Figure 2 that had

(31) Summerville, R. H.; Hoffmann, R. *J. Am. Chem. Soc.* **1979**, *101*, 382.

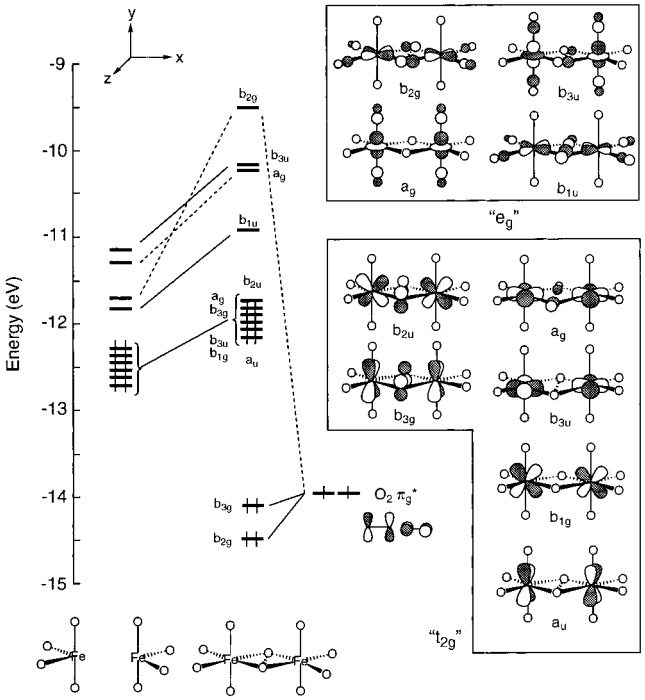

Figure 4. Orbital interaction diagram constructing the diiron peroxo model with a μ-η^2:η^2-O_2 core structure.

two such orbitals. The four nonbonding orbitals in the $Fe_2(H_2O)_8$ fragment lie at low energy, and play a significant role in the formation of a diiron peroxo complex with a μ-η^2:η^2-O_2 core.

All d-block orbitals of **2a** are shown in this illustration. The t_{2g} block of the composite complex is mostly made up of the iron d orbitals, as indicated, and the contribution from the ligand orbitals is small. Let us look at the metal−bridge interaction in detail. One of the π_g* orbital (π_g*(σ)) is in the Fe_2O_2 plane, and its partner (π_g*(p)) is perpendicular to that plane. The π_g*(σ) and π_g*(p) orbitals have good interactions with the d_{xz} and d_{xy} of Fe, respectively. Thus, the b_{2g} orbital is pushed up significantly to −10.2 eV, due to the strong out-of-phase interaction between the d_{xy} and π_g*(p) orbitals; the b_{3g} orbital at −12.3 eV remains almost unchanged, due to weak π-type interactions between the d_{xz} and π_g*(σ) orbitals, as shown in Figure 4.

Let us next take a look at the Walsh diagram (Figure 5) for the distortion from **2a** to **2b**. A similar diagram for $Mn_2(\mu$-$O)_2(H_2O)_8$, a system modeling the function of photosystem II, has been analyzed in detail.[23] The d-block orbitals remain unchanged along the reaction coordinate. The π_g* set (b_{3g} and b_{2u} in Figure 4) is also not changed dramatically by the distortion. In contrast, the b_{1u} level that is mainly composed of the σ_u* of dioxygen decreases significantly in energy as the O−O bond length is increased (small angles in Figure 5). The σ_u* of the peroxo form is located at −6 eV (outside the energy window of Figure 5). The b_{1u} symmetry of the σ_u* does not permit it to cross the "e_g" block orbitals, but allows a crossing of the "t_{2g}" block orbitals. Figure 5 looks a little different from Figure 3, but their essential points are similar—a crossing, real or avoided, of the metal valence orbitals by O−O σ_u*.

As the b_{1u} orbital comes down and crosses the "t_{2g}" block (when the dioxygen O−O bond length is increased), two electrons are transferred from the "t_{2g}" block to the b_{1u} orbitals, and the O−O bond is effectively cleaved. The change in the b_{1u} orbital from −11.2 to −14.7 eV is indicated in Scheme 6.

The calculated charges of one oxygen in **2a** and **2b** are −0.37 and −1.25, respectively. These values are a little smaller than

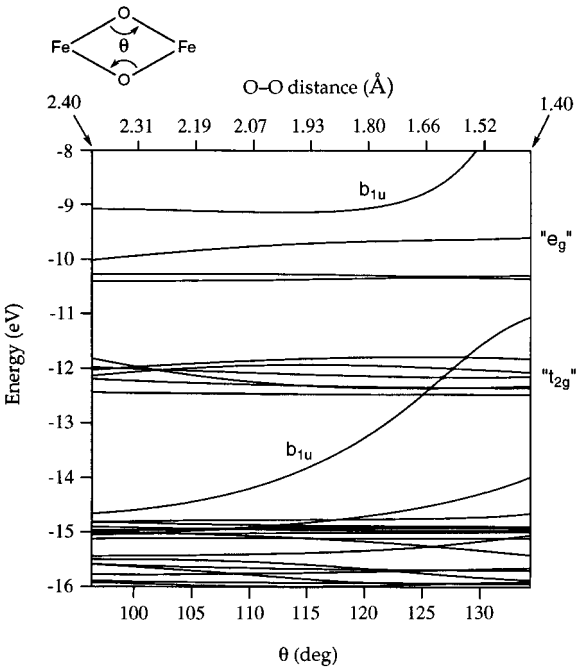

Figure 5. Walsh diagram for model **2a** as a function of O−O distance.

Scheme 6

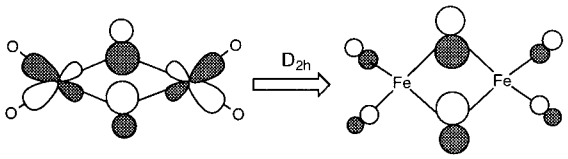

those of **1a** and **1b**, in spite of the same O−O bond distances. This difference is not due to the total charge difference between **1** (charge +3) and **2** (charge +4). In order to obtain more comparable total charges, we substituted water for the hydroxy bridge in **1a** and **1b** of Scheme 3, and recomputed the net charges. The calculated values for **1a′** and **1b′** (which have a water bridge) are −0.53 and −1.58, respectively. These values are comparable to −0.55 and −1.62 for **1a** and **1b**, which have a hydroxy bridge. We conclude that the μ-η^1:η^1-O_2 mode is more effective for electron transfer from the d-block orbitals to the dioxygen π_g* and σ_u*. We will show in the next section the reason why electron transfer is more significant in the Fe_2-(μ-η^1:η^1-O_2) complex. The O−O and Fe−O overlap populations and the net charges of O and Fe for **1a**, **1b**, **1a′**, **1b′**, **2a**, and **2b** are listed in Table 1. Although the net negative charges of the O atoms are greater in the end-on binding modes, i.e., **1a**/**1b** and **1a′**/**1b′** rather than in the side-on modes, **2a**/**2b**, the O−O overlap populations do not differ. The Fe−O bond is strengthened for the distortion from **2a** to **2b**, while it remains unchanged for the distortion from **1a** (**1a′**) to **1b** (**1b′**).

MOOP Analyses for Electron Transfer in Different O_2 Binding Modes

We analyzed molecular orbital overlap population (MOOP) diagrams[32] to see in detail how electron transfer occurs in our diiron−O_2 model complexes. These diagrams show graphically the contribution of various MOs to the overlap population. We show in Figure 6 the bonding and antibonding interactions between the two oxygen atoms in the diiron complexes, at O−O separations of 1.4 and 1.8 Å. Bonding overlap populations are plotted to the right and antibonding ones to the left. The dotted

(32) MOOP was introduced by Prosperio, D. M.; Mealli, C. in CACAO (a package of programs for extended Hückel molecular orbital analysis).

Table 1. Selected Overlap Populations and Atomic Net Charges for Models **1**, **1′**, and **2**

	overlap populations		net charges	
model	Fe−O	O−O	Fe	O
1a/**1b**	0.39/0.35	0.48/0.00	1.18/2.17	−0.55/−1.62
1a′/**1b′**	0.39/0.36	0.43/0.00	1.17/2.20	−0.53/−1.58
2a/**2b**	0.25/0.35	0.47/-0.01	1.28/2.11	−0.37/−1.25

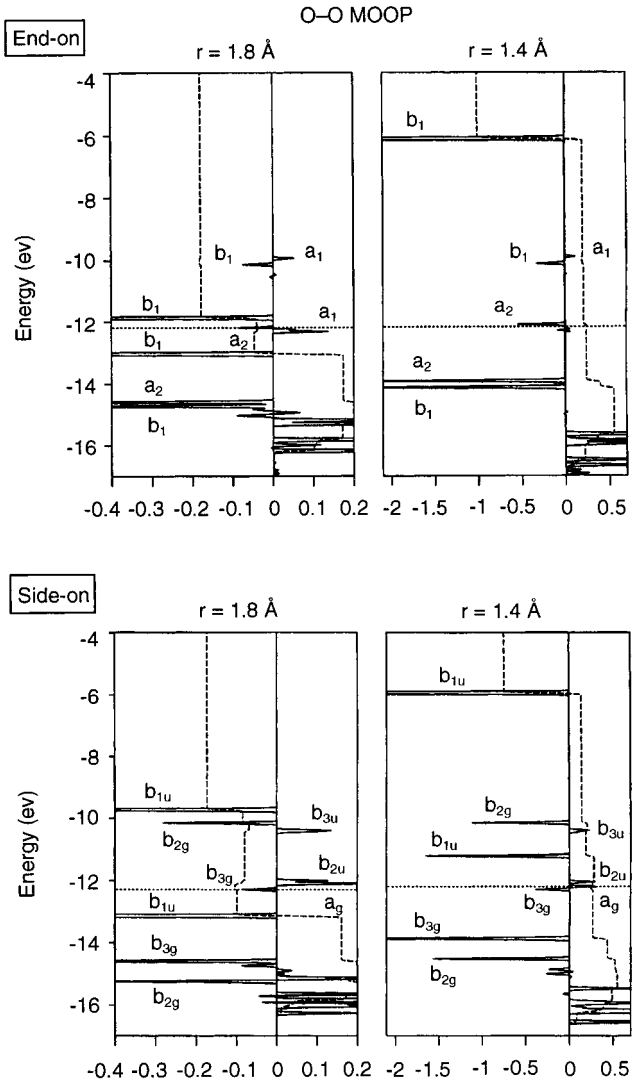

Figure 6. Molecular orbital overlap population (MOOP) analyses for the diiron−O_2 complexes with end-on and side-on binding modes. The O−O distances (r) are 1.4 and 1.8 Å. The dotted lines indicate the HOMO levels and the dashed lines running up the integrations of bonding and antibonding interactions. Note that the scales of the horizontal axes are different at the two distances.

lines mark the HOMO, and the dashed lines running up indicate integrations up to the indicated energy of all bonding and antibonding contributions. These graphs are essentially informative snapshots of the Walsh diagrams shown in Figures 3 and 5.

Let us first look at the end-on type binding mode with an O−O distance of 1.4 Å, i.e., the μ-η^1:η^1-O_2 mode. There are three main O−O antibonding orbitals, i.e., b_1 at −6 eV, a_2 at −14 eV, and b_1 at −14.2 eV, as shown in the upper, right illustration of Figure 6. The b_1 at −6 eV originates from the σ_u* of O_2 and the low-lying a_2 and b_1 from the π_g*. The strongly antibonding b_1 at −6 eV is unoccupied when the O−O distance is 1.4 Å, so that the net overlap population at the HOMO level is positive. This means that this peroxo species is still bound. As the O−O bond length is increased, the σ_u* goes down and crosses the HOMO at an O−O distance of about 1.8 Å, as indicated in the upper, left illustration of Figure 6. Now there is substantial antibonding below the HOMO level, as the dashed integrations indicate.

The features of the MOOPs for the side-on-type binding mode are a little different from those for the end-on-type binding mode, as shown in the lower illustrations of Figure 6. We can see four main O−O antibonding orbitals at the O−O distance of 1.4 Å, i.e., b_{1u} at −6 eV, b_{1u} at −11 eV, b_{3g} at −14 eV, and b_{2g} at −14.7 eV. The two b_{1u} orbitals derive mainly from the σ_u* of O_2 and both the b_{3g} and b_{2g} from the π_g*. Even when the O−O distance is increased to 1.8 Å, some orbitals containing oxygen character still remain above the HOMO level, in contrast to the end-on binding mode. This is also seen from Figures 2 and 4: the dioxygen π_u, π_g*, and σ_u* contribute to the unoccupied e_g-block orbitals of the $Fe_2(\mu$-η^2:η^2-$O_2)$ complex, whereas the same O_2 MOs do not contribute significantly to the e_g-block orbitals of the $Fe_2(\mu$-η^1:η^1-$O_2)$ complex. Therefore, electron transfer should be more substantial in the end-on binding mode rather than in the side-on mode, as seen from the calculated net charges of oxygen listed in Table 1.

It may appear that our calculational results are inconsistent with the observed Raman ν_{O-O} frequencies of ∼900 cm^{-1} in the end-on μ-η^1:η^1-O_2 mode and ∼800 cm^{-1} in the side-on μ-η^2:η^2-O_2 mode. However, we believe that the O−O stretching motion in the μ-η^2:η^2-O_2 mode is significantly coupled with the metal−metal stretch, as shown in Scheme 2. On the other hand, the O−O stretching in the μ-η^1:η^1-O_2 mode is nearly independent of the motion of the metals. Thus, the ν_{O-O} frequency in the μ-η^1:η^1-O_2 mode can be higher than that in the μ-η^2:η^2-O_2 mode.

Methane Activation by Oxoiron Species

Let us next consider the activation of methane at the diiron active sites. There has been much theoretical work on this subject.[33−39] However, to the best of our knowledge, a detailed reaction-path analysis for the conversion of methane to methanol has not yet been carried out in any catalytic system. Gas-phase reactions for the conversion of methane to methanol have been extensively studied (using ion cyclotron resonance mass spectrometry) in Schwarz's[40] and Armentrout's[41] laboratories. In a

(33) Saillard, J.-Y.; Hoffmann, R. *J. Am. Chem. Soc*. **1984**, *106*, 2006.
(34) (a) Perry, J. K.; Ohanessian, G.; Goddard, W. A., III. *J. Phys. Chem.* **1993**, *97*, 5238. (b) Perry, J. K.; Ohanessian, G.; Goddard, W. A., III. *Organometallics* **1994**, *13*, 1870.
(35) (a) Blomberg, M. R. A.; Siegbahn, P. E. M.; Svensson, M. *J. Am. Chem. Soc*. **1992**, *114*, 6095. (b) Siegbahn, P. E. M.; Blomberg, M. R. A. *Organometallics* **1994**, *13*, 354. (c) Siegbahn, P. E. M. *Organometallics* **1994**, *13*, 2833. (d) Siegbahn, P. E. M. *J. Am. Chem. Soc*. **1996**, *118*, 1487. (e) Siegbahn, P. E. M.; Crabtree, R. H. *J. Am. Chem. Soc*. **1996**, *118*, 4442.
(36) (a) Ziegler, T.; Tschinke, V.; Becke, A. D. *J. Am. Chem. Soc*. **1987**, *109*, 1351. (b) Ziegler, T.; Tschinke, V.; Fan, L.; Becke, A. D. *J. Am. Chem. Soc*. **1989**, *111*, 9177. (c) Ziegler, T.; Folga, E.; Berces, A. *J. Am. Chem. Soc*. **1993**, *115*, 636.
(37) (a) Koga, N.; Morokuma, K. *J. Phys. Chem*. **1990**, *94*, 5454. (b) Musaev, D. G.; Koga, N.; Morokuma, K. *J. Phys. Chem*. **1993**, *97*, 4064. (c) Musaev, D. G.; Morokuma, K.; Koga, N.; Ngyen, K.; Gordon, M. S.; Cundari, T. R. *J. Phys. Chem*. **1993**, *97*, 11435. (d) Musaev, D. G.; Morokuma, K. *J. Chem. Phys*. **1994**, *101*, 10697. (e) Musaev, D. G.; Morokuma, K. *J. Phys. Chem*. **1996**, *100*, 11600.
(38) (a) Sakaki, S.; Ieki, M. *J. Am. Chem. Soc*. **1991**, *113*, 5063. (b) Sakaki, S.; Ieki, M. *J. Am. Chem. Soc.* **1993**, *115*, 2373.
(39) (a) Cundari, T. R. *J. Am. Chem. Soc.* **1992**, *114*, 10557. (b) Cundari, T. R. *J. Am. Chem. Soc*. **1994**, *116*, 340.
(40) (a) Schröder, D.; Schwarz, H. *Angew. Chem., Int. Ed. Engl.* **1990**, *29*, 1433. (b) Schwarz, H. *Angew. Chem., Int. Ed. Engl.* **1991**, *30*, 820. (c) Schröder, D.; Fiedler, A.; Hrušák, J.; Schwarz, H. *J. Am. Chem. Soc.* **1992**, *114*, 1215.
(41) Chen, Y.-M.; Clemmer, D. E.; Armentrout, P. B. *J. Am. Chem. Soc.* **1994**, *116*, 7815.

Scheme 7

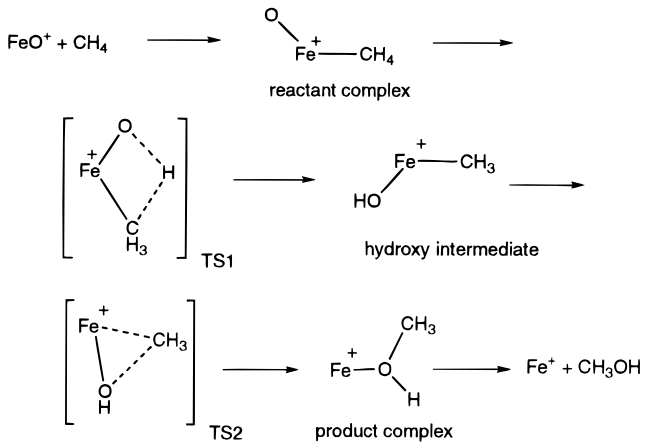

recent paper,[42] Yoshizawa et al. have analyzed possible reaction pathways for the conversion of methane to methanol catalyzed by FeO^+ using a hybrid (Hartree−Fock/density-functional) method. The preferred reaction pathway calculated includes an important insertion intermediate, $HO-Fe^+-CH_3$, as shown in Scheme 7.

The activation energies from the reactant complex to the hydroxy intermediate via TS1 are computed to be 30−40 kcal/mol.[42] Although TS1 is concerned with a C−H bond cleavage step, these values are rather small compared to a C−H bond energy of ∼100 kcal/mol. Another interesting point in this proposed reaction pathway is that the Fe−O distance does not change significantly throughout (1.6−1.7 Å), except for the product complex that has an Fe−O distance of 2.0 Å. This shows that an Fe−O• radical is unlikely to contribute to the reaction pathway in Scheme 7.

These reactions of methane are initiated by formation of an FeO^+−methane complex that has an intriguing five-coordinate carbon species. The important orbital interactions that weaken the C−H bonds of the coordinated methane are those between the methane HOMO and the d-block orbitals of FeO^+. The reactant complex, with an interesting $Fe-CH_4$ bond length of 2.1−2.2 Å, plays an important role in the initial stage of methane activation. The methane moiety in the reactant complex (in Scheme 7) is calculated to have a C_{3v}-type geometry. This structure is found from our vibrational analyses to correspond to a true minimum on a potential energy surface. The reaction pathway indicated in Scheme 7 includes concerted hydrogen and methyl migrations that lead to the final product, i.e., methanol. Although we cannot easily compare the simpler gas-phase reaction with the enzymatic ones, we think that the concerted mechanism of Scheme 7 may play a role in the catalytic cycle of the metalloenzyme system. Our proposal argues strongly against the widely accepted oxygen rebound mechanism mentioned above.

Shestakov and Shilov[43] have proposed that the activation of hydrocarbons proceeds through interactions between the ferryl active center and hydrocarbons. In the initial stage of the reaction, their model also postulates a C_{3v}-type deformation of hydrocarbons, as indicated in the middle of Scheme 8. However, this mechanism differs from the one we found in Scheme 7, in that the mechanism of Shestakov and Shilov[43] suggests that the carbon atom of C_{3v}-deformed hydrocarbons coordinates

Scheme 8

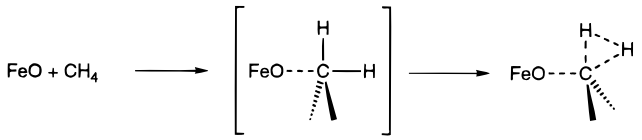

Scheme 9

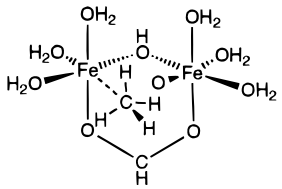

directly to the ferryl "oxygen". Shteinman[44] proposed the $Fe_2(\mu\text{-}O)_2$ core for **Q** and discussed its reactivity toward methane in a way similar to Scheme 8. To the extent that we can trust our calculations, this type of coordination appears to be unlikely; it does not correspond to a stationary point (minimum or saddle) on a potential energy surface.

Newcomb and Hollenberg and their co-workers[45] inferred from a measured short radical lifetime of 70 fs that in alkane hydroxylation by cytochrome P450 hydrogen atom abstraction does not occur with a linear C−H−O array that is assumed in the oxygen rebound mechanism but via a "side-on" approach of oxygen to the C−H bond. Chan and Floss and their collaborators[46] proposed (using as a probe ethane bearing a chiral methyl group) a concerted mechanism for ethane hydroxylation by a particular form of MMO, i.e., one proceeding through a five-coordinate carbon species. However, they have not yet determined experimentally whether this initially formed species has a C−O or a C−metal bond. The reaction mechanism in so-called *Gif* chemistry proposed by Barton and collaborators[47] rejects the typical radical-based mechanisms, on the basis of the selectivity for hydroxylation and ketonization of alkanes. Moreover, Floss and Lipscomb et al.[7] and Lippard et al.[48] reported that the product alcohol displayed 65−72% retention of stereochemistry at the labeled carbon for the ethane substrate and 77% retention for butanes labeled at the primary carbon. Newcomb and Lippard et al.[49] recently suggested a nonsynchronous concerted mechanism for hydroxylations by MMO via possible formation of a five-coordinate carbon species and pseudorotation. The work of these research groups[7,45−49] is encouraging for our theoretical studies.

We have discussed the importance of the C_{3v} deformation for methane (proposed by Shestakov and Shilov[43]) from the point of view of second-order perturbation theory.[14] We concluded from qualitative calculations that a C_{3v}-deformed methane can be theoretically activated on a supposed diiron active site of MMO, if that site includes a five-coordinate iron active center, as shown in Scheme 9. Our proposals include a complex with an interesting $Fe-CH_4$ bond in the initial stage of the catalytic cycles, just as in Scheme 7. In the context of

(42) Yoshizawa, K.; Shiota, Y.; Yamabe, T. *Chem. Eur. J.* **1997**, *3*, 1160.
(43) Shestakov, A. F.; Shilov. A. E. *Zh. Obshch. Khim.* **1995**, *65*, 60; *J. Mol. Catl. A* **1996**, *105*, 1.
(44) Shteinman, A. A. *Izv. Akad. Nauk. Ser. Khim.* **1995**, 1011; *Russ. Chem Bull.* **1995**, *44*, 975.
(45) Newcomb, M.; Le Tadic-Biadatti, M.-H.; Chestney, D. L.; Roberts, E. S.; Hollenberg, P. F. *J. Am. Chem. Soc.* **1995**, *117*, 12085.
(46) Wilkinson, B.; Zhu, M.; Priestley, N. D.; Nguyen, H.-H. T.; Morimoto, H.; Williams, P. G.; Chan, S. I.; Floss, H. G. *J. Am. Chem. Soc.* **1996**, *118*, 921.
(47) Barton, D. H. R.; Doller, D. *Acc. Chem. Res.* **1992**, *25*, 504.
(48) Valentine, A. M.; Wilkinson, B.; Liu, K. E.; Komar-Panicucci, S.; Priestley, N. D.; Williams, P. G.; Morimoto, H.; Floss, H. G.; Lippard, S. J. *J. Am. Chem. Soc.* **1997**, *119*, 1818.
(49) Choi, S. Y.; Eaton, P. E.; Hollenberg, P. F.; Liu, K. E.; Lippard, S. J.; Newcomb, M.; Putt, D. A.; Upadhyaya, S. P. Xiong, Y. *J. Am. Chem. Soc.* **1996**, *118*, 6547.

Scheme 10

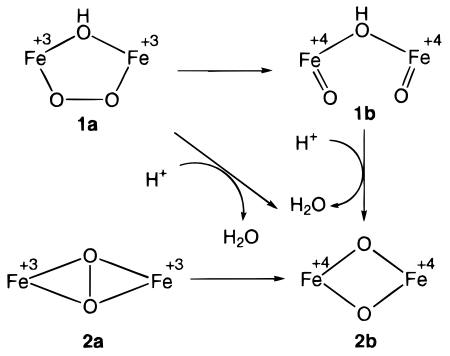

recent organometallic chemistry, a five-coordinate carbon species is not that unrealistic.[50] Previous orbital interaction analyses[14] have shown that interactions between the methane t_2 HOMO (C−H bonding) and the unoccupied d-block orbitals of MMO model complexes (rather than the interactions between the LUMO (C−H antibonding) and the occupied d-block orbitals) play an essential role in activating the methane C−H bonds. Our extended Hückel calculations suggested that a six-coordinate iron is not likely to possess direct reactivity with methane, even if it contains an active ferryl species, but that methane can be activated if a coordinatively unsaturated metal center, e.g., a five-coordinate iron is generated. The structure in Scheme 9 is, of course, one such possibility.[14]

Methane−Methanol Conversion on Diiron Active Sites

Having described a basic concept for methane activation in our previous work, let us next look at the coordination of methane to a supposed active site that can model intermediate **Q** of MMO. How **Q** interacts with methane is the key to understanding of this enzyme. From recent EXAFS and Mössbauer analyses, **Q** is proposed to have an $Fe_2(\mu\text{-}O)_2$ diamond core and the two Fe(IV) centers are likely to have a coordination number no higher than 5.[24] The experimentally proposed five-coordinate iron active centers in the diamond core are consistent with what is theoretically needed from our discussion.[14] The diamond core is not symmetric; each iron has one short (1.77 Å) and one long (2.05 Å) Fe−O bonds and the Fe−Fe distance is rather short, 2.46 Å. We assume that such a diamond core is involved in intermediate **Q** although other structures are possible.[8b]

One of our models (**2b**), which is similar to the proposed diamond core of intermediate **Q**, can be created directly from **1a**, **1b**, and **2a**, as shown in Scheme 10. In any case, O−O bond cleavage occurs in forming **2b**. We have discussed in the previous sections how the O−O bonds of various peroxo intermediates might be cleaved. Peroxo model complexes of type **1a**[10,11] and of a modified *trans*-μ-1,2-O_2 mode[12] have been synthesized and characterized, but the diiron peroxo form of type **2a** has not yet been observed in actual or model enzyme systems, in contrast to dicopper systems. The actual intermediate **P** of MMO is supposed from its Raman spectrum[8] to include end-on core structures. So we think that the reaction pathway **1a** → (**1b**) → **2b** is plausible.

Let us now suppose that a dioxo complex of type **2b** is formed. For calculations, we assume here an $Fe^{IV}-Fe^{IV}$ core structure, which has been proposed by Lipscomb and Münck and their collaborators[51] to be in the actual intermediate **Q** of MMO. Moreover, we assume that both the irons are five-coordinated, along the line of recent work,[24] although four-coordinate iron models are also possible. We then approach a C_{3v}-distorted methane to one of the iron centers, in order to look at whether or not the methane is bound to the supposed active site. We believe from our earlier theoretical studies[14,42] that an initially formed species should contain an $Fe-CH_4$ bond, not an $O-CH_4$ bond.

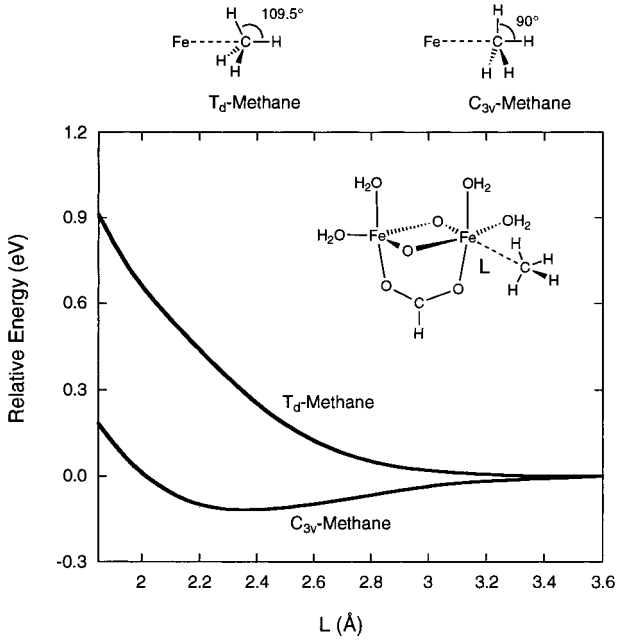

Figure 7. Total energy diagrams for the coordination of T_d- and C_{3v}-type methanes to a supposed diiron active site of intermediate **Q** in an η^3-binding mode as a function of Fe···C distance *L*.

The energetics of coordination of the T_d methane and a C_{3v}-distorted methane to the supposed active site of intermediate **Q** of MMO is shown as a function of Fe···C distance (*L*) in Figure 7. In these calculations, we reverted to a carboxylate (formate) bridging ligand instead of two water ligands in **2b**. The interaction between the T_d methane (with equivalent H−C−H angles of 109.5°) and the model active site is repulsive, but that between a C_{3v}-distorted methane and the active site is clearly attractive. The computed binding energy of a C_{3v} methane (with three H−C−H angles of 90°) is ∼0.1 eV in this model (at L = 2.35 Å), consistent with our previous calculations[14] based on models that are a little different. Methane is thus weakly bound at the five-coordinate iron center of a model of intermediate **Q**, as indicated in the illustration in Figure 7. The binding energy is small, but given the frozen geometries and our previous studies, we think that it is very much indicative of activation.

The coordination of a C_{3v}-distorted methane that we have discussed above is one possibility, denoted as an η^3-binding mode. There is another possible coordination for methane, which we call an η^2-binding mode, as shown in Scheme 11. The two binding modes were found in calculations on the OFe^+-(CH_4) complex, both minima on a potential energy surface from density-functional calculations.[42,52] Koga and Morokuma[37a] calculated with the ECP (effective core potential) method that the η^2-binding mode is 4 kcal/mol more stable than the η^3-binding mode in the methane-$RhCl(PH_3)_2$ complex.

Piers and co-workers[50] recently found the η^2-binding mode in a Zr complex that includes a five-coordinate carbon species from X-ray structural analyses. The H−C−H angle in the vicinity of the metal active center is opened up as theoretically

(50) Spence, R. E. v. H.; Parks, D. J.; Piers, W. E.; MacDonald, M. A.; Zaworotko, M. J.; Rettig, S. J. *Angew. Chem., Int. Ed. Engl.* **1995**, *34*, 1230.
(51) Lee, S.-K.; Fox, B. G.; Froland, W. A.; Lipscomb, J. D.; Münck, E. *J. Am. Chem. Soc.* **1993**, *115*, 6450.
(52) Yoshizawa, K.; Shiota, Y.; Yamabe, T. Submitted for publication.

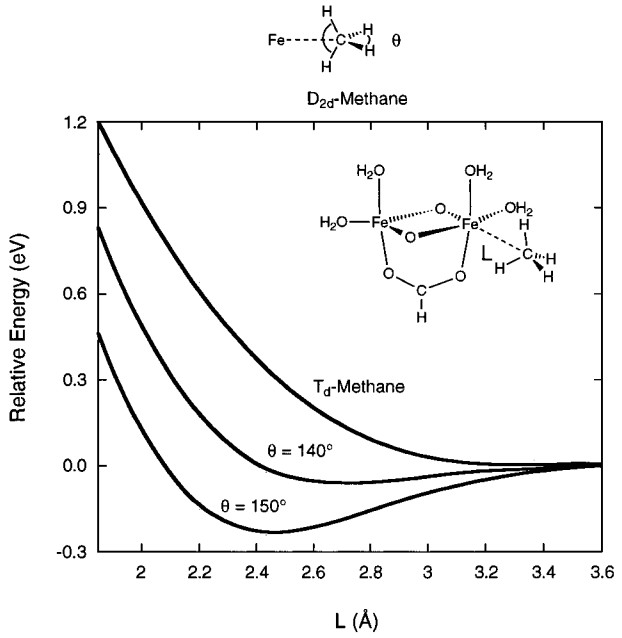

Figure 8. Total energy diagrams for the coordination of T_d- and D_{2d}-type methanes to a supposed diiron active site of intermediate **Q** in an η^2-binding mode as a function of Fe···C distance L.

expected: it was computed to be 120° in the $OFe^+(CH_4)$ complex discussed above, and a corresponding B−C−B angle in the Zr complex[50] was determined to be 149°. Thus, methane coordinated in the η^2-binding mode would have D_{2d} (more precisely C_{2v}) symmetry. Radius et al.[53] have recently analyzed the electronic structure of such a distorted five-coordinate carbon species from the viewpoint of orbital interactions.

Let us look at the interaction between a D_{2d}-distorted methane and a model of intermediate **Q** of MMO. The total energy diagrams for the coordination of the T_d methane and D_{2d}-distorted methanes to the supposed active site are shown in Figure 8. The interaction between a D_{2d}-distorted methane and the active site is attractive also in this binding mode, but that between the T_d methane and the active site is repulsive. The computed binding energy of a D_{2d} methane (with two H−C−H angles opened up to 150°) is about 0.15 eV in this model (at L = 2.4 Å), consistent with the calculational result based on a different model with an η^3-binding mode in Figure 7. Methane is thus bound at the five-coordinate iron center of a model of intermediate **Q** both in the η^2-binding mode as well as in the η^3-binding mode.

From the viewpoint of known catalytic chemistry (as well as from that of perturbation theory), it is in general reasonable to assume that catalytically active metal complexes might be coordinatively unsaturated. Thus, we think that a four-coordinate iron would activate methane in a similar manner. The C−H bonds of methane are activated in these complexes because of significant electron transfer from the methane t_2 HOMO (C−H bonding) to the unfilled d-block orbitals of the iron complex. In fact, the computed total charge of the methane is +0.18 in the complex with an η^3-binding mode in Figure 7 (at L = 2.35 Å) and +0.28 in the complex with an η^2-binding mode in Figure 8 (at L = 2.4 Å). The reader can see detailed analyses of the orbital interactions that cause significant electron transfers in our previous paper.[14]

By analogy to the calculated mechanism for the gas-phase reaction shown in Scheme 7, we can propose possible mechanisms for the methane−methanol conversion on the diiron active site of a model complex for intermediate **Q**, shown in Figure 9. Two-step concerted mechanisms that include hydrogen and methyl migrations will lead to the formation of the product complex, followed by dissociation to the final product methanol. The initially formed species would exhibit an η^3- or η^2-CH_4 mode, as shown in Scheme 11, depending on coordination sphere.

Our concerted mechanisms are likely to afford retention of stereochemistry at the carbon center of methane. However, as recently suggested by Lippard et al.,[48] if a certain distortion occurs at a five-coordinate carbon species, we can understand the reason why partial inversion of stereochemistry at a labeled carbon center is observed in alkane hydroxylation by MMO. Our basic idea differs from the models proposed by Newcomb and Lippard et al[45,48,49] because we believe that an initially formed species has an Fe−CH_4 bond,[14] not an O−CH_4 bond. As discussed below, D_{2d} deformation of the hydrocarbon in the η^2-binding mode may play a significant role in the inversion at a carbon center compared to a C_{3v} deformation in the η^3-binding mode, although the two binding modes are close in energy.

Let us first consider a Berry pseudorotation at a five-coordinate carbon species with an η^3-binding mode to look at whether or not it can invert the carbon center of coordinated methane. As shown in Scheme 12, the first step of this pseudorotation is a "T_d-to-C_{3v}" distortion of the coordinated methane (**a** → **b**); the second step is an opening of the H−C−H angle roughly from 120° to 180° (**b** → **c**); and the third is a closing of the Fe−C−H angle from 180° to 120° (**c** → **d**). However, such simple processes are found not to invert the carbon center.

In contrast, inversion of the carbon center is easily attained in the η^2-binding mode, as shown in the lower of Scheme 12. This type of distortion through a planar (for CH_4) structure has been extensively discussed for free methane at different levels of theory;[54] most recent high-level multiconfigurational computations estimate the barrier height to be 117.0 kcal/mol.[54j] We expect that the energy barrier is significantly decreased in a methane coordinated to a metal center, compared with free methane, due to significant electron transfer from the coordinated methane to the diiron complex.

Figure 10 shows the potential energy diagrams along the assumed reaction coordinate for free methane and the methane coordinated in an η^2 manner to a model active site of intermediate **Q**. Methane is inverted from the T_d structure with H−C−H angles of 109.5° through a planar D_{4h} structure while retaining D_{2d} symmetry along the reaction coordinate. The energy requirement forcing free methane from its T_d structure toward a planar D_{4h} structure was calculated to be 125 kcal/mol with the approximate extended Hückel method. This value is consistent with 117 kcal/mol from high-level multiconfigurational calculations.[54j]

The activation energy for such an inversion at the five-coordinate methane with an η^2-binding mode was calculated to be 81 and 62 kcal/mol at the Fe−C distance of 2.4 and 2.0 Å, respectively. These values are remarkably smaller than the 125

(53) Radius, U.; Silverio, S. J.; Hoffmann, R.; Gleiter, R. *Organometallics* **1996**, *15*, 3737.

(54) (a) Pople, J. A.; Santry, D. P.; Segal, G. A. *J. Chem. Phys.* **1965**, *43*, S129. (b) Hoffmann, R.; Alder, R. W.; Wilcox, C. F., Jr. *J. Am. Chem. Soc.* **1970**, *92*, 4992. (c) Durmaz, S.; Murrell, J. N.; Pedley, J. B. *J. Chem. Soc., Chem. Commun*. **1972**, 933. (d) Firestone, R. A. *J. Chem. Soc., Chem. Commun.* **1973**, 163. (e) Collins, J. B.; Dill, J. D.; Jemmis, E. D.; Apeloig, Y.; Schleyer, P. v. R.; Seeger, R.; Pople, J. A. *J. Am. Chem. Soc.* **1976**, *98*, 5419. (f) Hehre, W. J.; Stewart, R. F.; Pople, J. A. *J. Chem. Phys*. **1969**, *51*, 2657. (g) Hariharan, P. C.; Pople, J. A. *Theor. Chim. Acta* **1973**, *28*, 213. (h) Krogh-Jespersen, M. -B.; Chandrasekhar, J.; Würthwein, E.-H.; Collins, J. B.; Schleyer, P. v. R. *J. Am. Chem. Soc.* **1980**, *102*, 2263. (i) Crans, D. C.; Snyder, J. P. *J. Am. Chem. Soc.* **1980**, *102*, 7152. (j) Gordon, M. S.; Schmidt, M. W. *J. Am. Chem. Soc.* **1993**, *115*, 7486.

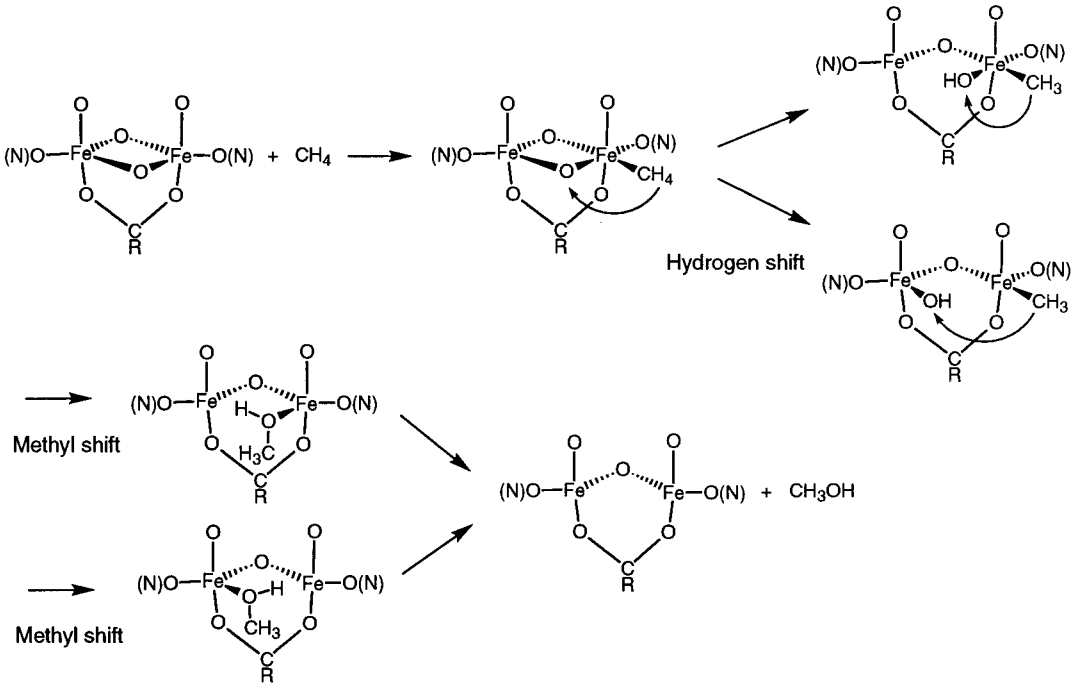

Figure 9. Possible concerted mechanisms for the conversion of methane to methanol on the diiron active site of MMO.

Scheme 11

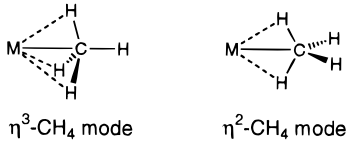

Scheme 12

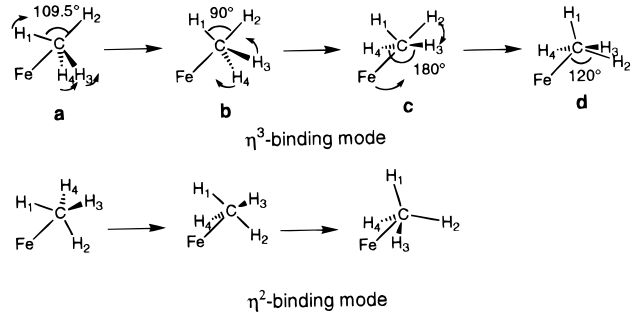

kcal/mol for free methane. The result could be just a shortcoming of the extended Hückel method. However, our general experience is that a reduction in the activation energy from methane of the magnitude calculated is a real signal of a new mechanism at work. We therefore think that inversion of stereochemistry can reasonably occur in a five-coordinate carbon species that we have proposed to be formed in the initial stage of the reaction of methane with the diiron active site of intermediate **Q**.

Of course, we need to perform detailed theoretical analyses, with better computational methods, on the mechanism for alkane hydroxylation on the MMO active site. Recent theoretical work of high quality by Siegbahn and Crabtree[55] for the mechanism of C−H activation on MMO models, however, leads to a radical mechanism that includes a direct H atom abstraction from the substrate methane, quite different from our two-step concerted mechanisms.[56]

Since there is at present no clear-cut explanation of the nature of the mechanism for the conversion of methane to methanol

(55) Siegbahn, P. E. M.; Crabtree, R. H. *J. Am. Chem. Soc*. **1997**, *119*, 3103.

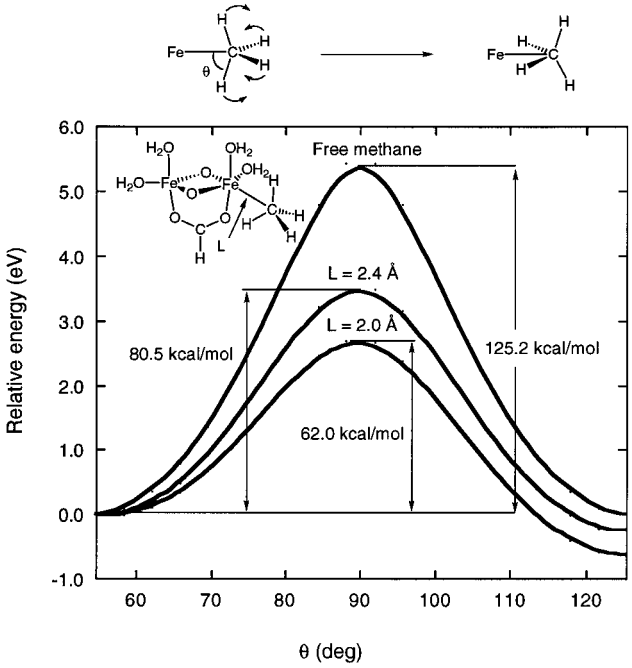

Figure 10. Activation energies for the inversion of free methane and five-coordinate methane along a supposed reaction coordinate.

on the diiron active site, we will delay further discussion at this time. However, we think that concerted reactions can occur on the diiron active site under physiological conditions, and that such mechanisms may be more favorable than widely accepted radical-based mechanisms. In a future study we will examine possible reaction pathways for the conversion of methane to methanol on supposed non-heme diiron models of MMO.

Conclusions

Dioxygen O−O bond cleavage is a crucial step in the catalytic cycles of non-heme diiron metalloenzymes. We discuss such

(56) From DFT calculations an H atom abstraction on a diiron model complex of intermediate **Q** was confirmed to occur through a four-centered transition state just like TS1 in Scheme 7. Yoshizawa, K.; Ohta, T.; Shiota, Y.; Yamabe, T. *Chem. Lett.*, in press.

Table 2. Extended Hückel Parameters For Fe, O, C, and H Atoms

orbital	H_{ii} (eV)	ζ_{i1}	c_1	ζ_{i2}	c_2
Fe4s	−9.1	1.9			
Fe4p	−5.32	1.9			
Fe3d	−12.6	5.35	0.5505	2.00	0.6260
O2s	−32.3	2.275			
O2p	−14.8	2.275			
C2s	−21.4	1.625			
C2p	−11.4	1.625			
H1s	−13.6	1.3			

cleavage in several diiron model complexes with different O_2 binding modes. We analyze qualitatively the electronic structure of peroxo and dioxo complexes on the basis of FMO, Walsh, and MOOP analyses. From the point of view of charge transfer from the d-block orbitals to the bound dioxygen, we think that the μ-η^1:η^1-O_2 mode might be more effective than the μ-η^2:η^2-O_2 mode in the cleavage of dioxygen O−O bond.

Moreover, we suggest that a specific five-coordinate iron complex modeling intermediate **Q** might react directly with methane. Extended Hückel calculations indicate that a C_{3v}- or D_{2d}-distorted methane can be theoretically activated or coordinated if a coordinatively unsaturated iron is generated in a non-heme diiron model complex. Significant electron transfer occurs from methane to the diiron active site through interactions between the methane t_2 HOMO and the unoccupied d-block orbitals. This differs from the formation of a peroxo species, a process in which significant electron transfer occurs from the d-block to the bound dioxygen. We propose a novel two-step concerted mechanism that includes hydrogen and methyl migrations for alkane hydroxylation by the supposed active site of MMO. We suggest that inversion of methane through a planar D_{4h} structure might occur at a five-coordinate carbon species, the initially formed complex of methane and intermediate **Q**. Such an inversion of methane coordinated to a model complex is significantly easier than in free methane, due to significant electron transfer. This mechanism may explain observed inversion of stereochemistry at a labeled carbon center in alkane hydroxylation by MMO. These new results are based on our previous predictions in ref 14.

Acknowledgment. The work in Kyoto was supported by a Grant-in-Aid for Scientific Research from the Ministry of Education, Science and Culture of Japan and by "Research for the Future" Program from the Japan Society for the Promotion of Science (JSPS-RFTF96P00206). R.H. thanks the National Science Foundation (CHE-9408455) for its support of this work.

Appendix

Extended Hückel calculations were carried out using *YAeHMOP* (Yet Another Extended Hückel Molecular Orbital Package);[30] parameters used for iron, oxygen, carbon, and hydrogen appear in Table 2.

We have extensively used FMO (fragment molecular orbital), Walsh, and MOOP (molecular orbital overlap population) analyses in this paper. Partition of a molecular orbital into two or more FMOs is a very useful way of looking at important orbital interactions in a molecule. We do not need to know the details of the electronic structures of fragments; it is sufficient that we look at the frontier orbitals of fragments and their reconstructions. The theoretical background of the FMO method lies in perturbation molecular orbital theory.[57] A diagram that shows how the MO levels of a molecule vary as a function of geometrical change is known as a Walsh diagram. A major function of a Walsh diagram is to account for the structural regularity observed for a series of closely related molecules with the same number of valence electrons, and such a diagram is also useful in understanding a variety of electronic properties of molecules. What an MOOP diagram plots is the contribution of individual orbitals to the total overlap population. Note that the horizontal scale of MOOP diagrams is arbitrary: the peak heights or integrations of MOOPs for different bond types are not comparable.

JA9726419

(57) Albright, T. A.; Burdett, J. K.; Whangbo, M.-H. *Orbital Interactions in Chemistry*; Wiley: New York, 1985.